RESEARCH PAPER

PCCP
www.rsc.org/pccp

The orientational order and conformational distributions of the two enantiomers in a racemic mixture of a chiral, flexible molecule dissolved in a chiral nematic liquid crystalline solvent

James W. Emsley,*[a] Philippe Lesot[b] and Denis Merlet[b]

[a] *Department of Chemistry, University of Southampton, Southampton, UK SO17 1BJ. E-mail: J.W.Emsley@soton.ac.uk; Fax: 44 (0)2380 593781; Tel: 44 (0)2380 592156*

[b] *Laboratoire de Chimie Structurale Organique, Université de Paris-Sud, CNRS UMR 8074, ICMMO, Bât. 410, 91405, Orsay cedex, France. E-mail: philesot@icmo.u-psud.fr; denismerlet@icmo.u-psud.fr; Fax: 33 (0)1 69 15 47 70; Tel: 33 (0)1 69 15 47 59*

Received 9th October 2003, Accepted 3rd December 2003
First published as an Advance Article on the web 6th January 2004

The orientational order and conformational distributions of the two enantiomers of (±)-α-ethylhexanoic acid-d_{15}, a flexible chiral molecule, dissolved in a chiral nematic liquid crystalline solvent made of PBLG in an organic co-solvent are obtained by analysis of NMR data. The anisotropic, NMR parameters are obtained from the separated analysis of the two enantiomers using carbon–deuterium, deuterium–deuterium 2D correlation experiments and proton-coupled carbon-13 1D experiments. The analysis of conformational distributions, and the conformationally dependent orientational order parameters are derived using the additive potential, AP, model.

Introduction

The two enantiomers in a racemic mixture give different NMR spectra when dissolved in a chiral, nematic solvent, such as solutions of poly-γ-benzyl-L-glutamate (PBLG) or poly-ε-carbobenzyloxy-L-lysine (PCBLL) in organic solvents.[1,2] This phenomenon has been exploited in non-racemic mixtures for the determination of enantiomeric excess, and here there is an advantage over other methods of the wide variety of chemical and structural types which can be studied.[3,4] The basic phenomenon which provides the enantiomeric discrimination is that two enantiomers have different molecular orientational order, and hence the averages, $\left\langle A_{20}^{\boldsymbol{B}_o,R}\right\rangle$ and $\left\langle A_{20}^{\boldsymbol{B}_o,S}\right\rangle$, of the components along the applied static magnetic field, $\mathbf{B}_o$, of a second-rank interaction are different. Thus, for a rigid molecule[5]

$$\left\langle A_{20}^{\boldsymbol{B}_o,R}\right\rangle = A_0^R + \frac{2}{3}\sum_{\alpha,\beta} S_{\alpha\beta}^R A_{\alpha\beta}^R \qquad (1)$$

where $S_{\alpha\beta}^R$ is the second-rank orientational order parameter for the enantiomer *R*. A_0^R is the isotropic average, and $A_{\alpha\beta}^R$ are the components of the tensor $\mathbf{A}^R$ in molecule-fixed axis (*x*,*y*,*z*). If values of $A_{\alpha\beta}^R$ are known, then measurement of at least five values of $\left\langle A_{20}^{\boldsymbol{B}_o,R}\right\rangle - \mathrm{A}_0^R$ are sufficient to determine the order matrix $\mathrm{S}_{\alpha\beta}^R$, and similarly for the *S* enantiomer. Measurements of both $\mathrm{S}_{\alpha\beta}^S$ and $\mathrm{S}_{\alpha\beta}^R$ have been made for some pairs of rigid enantiomers, and these have shown that the differences in the values of $\left\langle A_{20}^{\boldsymbol{B}_o,R}\right\rangle$ and $\left\langle A_{20}^{\boldsymbol{B}_o,S}\right\rangle$ can be accounted for by differences only in the order matrices.[6]

For non-rigid molecules the relationship between $\left\langle A_{20}^{\boldsymbol{B}_o,R}\right\rangle$ and $\left\langle A_{20}^{\boldsymbol{B}_o,S}\right\rangle$ and the orientational order is more complex. A non-rigid molecule is defined here as having an exchange between different conformations which is fast compared with the changes this motion produces in values of $\left\langle A_{20}^{\boldsymbol{B}_o,R}\right\rangle$ and $\left\langle A_{20}^{\boldsymbol{B}_o,S}\right\rangle$. For such fast motion the observed averages along the static magnetic field direction, $\left\langle A_{20}^{\boldsymbol{B}_o,R}\right\rangle_\phi$ and $\left\langle A_{20}^{\boldsymbol{B}_o,S}\right\rangle_\phi$, depend on how the molecules move relative to $\boldsymbol{B}_o$, and the details of the intra-molecular motion, the latter symbolized by the subscript ϕ. Eqn. (1) is now replaced by[7]

$$\left\langle A_{20}^{\boldsymbol{B}_o,R}\right\rangle_\phi = \int P_{\mathrm{LC}}^R(\phi_i) A_0^R(\phi_i)\mathrm{d}\phi_i + \frac{2}{3}\int P_{\mathrm{LC}}^R(\phi_i) A_{\alpha\beta}^R(\phi_i) S_{\alpha\beta}^R(\phi_i)\mathrm{d}\phi_i \qquad (2)$$

where $P_{\mathrm{LC}}^R(\phi_i)$ is the probability that the *R* enantiomer is in a conformation defined by a set of bond rotation angles ϕ_i. The interaction tensor components will obviously depend on ϕ_i, but perhaps less obviously so too do the components of the order tensor.

The main question addressed in this work is whether the conformational distribution functions $P_{\mathrm{LC}}^R(\phi_i)$ and $P_{\mathrm{LC}}^S(\phi_i)$, and the order parameters $S_{\alpha\beta}^R(\phi_i)$ and $S_{\alpha\beta}^S(\phi_i)$, can be derived from NMR data obtained on chiral flexible molecules dissolved in a PBLG nematic liquid crystalline solvent. The molecule chosen for study is α-ethylhexanoic acid in racemic mixture (denoted here (±)-EHA), primarily because of the ease of synthesis of a sample deuterated at all sites except the acid, position 26, thus yielding values of the quadrupolar splittings, $\Delta\nu^R$ and $\Delta\nu^S$ at positions 11–25. The numbering of the atoms in the molecules is displayed in Fig. 1.

Experimental

Synthesis

The deuterated (±)-EHA ((±)-EHA-d_{15}) was synthesized by a catalytic deuterium exchange method using D_2O in a slightly alkaline condition at high temperature and pressure.[8] The experimental procedure can be found in ref. 9. The level of deuteriation was found by proton NMR to be ~90%.

DOI: 10.1039/b312512b

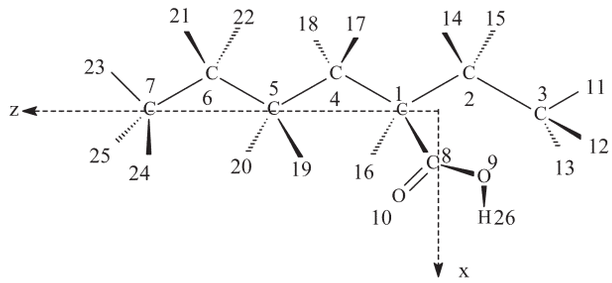

Fig. 1 Numbering of atoms of (±)-EHA used in this work and definition of axes (*x*,*y*,*z*) of the reference molecular frame. The molecular frame is orthonormal, with *y* normal to the *xz* plane.

NMR spectroscopy

The chiral liquid crystalline NMR samples of the perdeuterated and protonated EHA in racemic mixture were prepared identically using 100 mg of PBLG (commercially available from Sigma-Aldrich) with a MW ~112 000, 50 mg of (±)-EHA, and 350 mg of $CHCl_3$, the organic co-solvent, directly weighed into a 5 mm od NMR tube. Various theoretical and experimental details of the method can be found in refs. 1 and 4. The NMR experiments were performed at 9.4 T on a Bruker DRX 400 high-resolution spectrometer equipped with an inverse triple nuclei probe (TXI), or a broadband probe (BBI), operating at 61.4 MHz for deuterium and 100.6 MHz for carbon-13. The temperature of the samples was maintained at 300 K (BVT 3200) and the tubes were not spun during acquisition. The effects on the spectra of the proton–deuterium scalar and dipolar couplings in the molecule were removed by proton broadband decoupling using the WALTZ-16 sequence. For the carbon–deuterium correlation 2D experiment shown below, the deuterium channel (lock) of the probe was used. All 2D experiments were zero-filled to 1024 (t_1) × 2048 (t_2) data points prior to the double Fourier transformation. Other experimental NMR parameters or details are given in the figure captions.

Results and discussions

Spectral analysis

The proton-decoupled 1D deuterium spectrum of a sample of the (±)-EHA-d_{15} dissolved in the PBLG/$CHCl_3$ phase and recorded at 300 K is shown in Fig. 2. This 1D spectrum is a superposition of the deuterium signals given from each enantiomer, and the main task for the spectrum analysis is to obtain the quadrupolar splittings, $\Delta\nu_{CD_i}$, for the deuterium nuclei at each position in each enantiomer.

The first step consists of identifying the two components of each quadrupolar doublet, and to assign them to their position in the molecule. This was achieved using a ^2H–^{13}C HETCOR 2D experiment which correlates the deuterium and proton-decoupled ^{13}C spectra, as shown in Fig. 3.[9] The ^{13}C–{^1H}

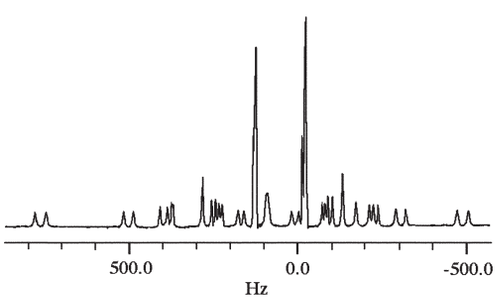

Fig. 2 61.4 MHz ^2H–{^1H} 1D spectrum of the (±)-EHA-d_{15} dissolved in the PBLG/$CHCl_3$ phase at 300 K using a simple one-pulse sequence. A Gaussian filtering (LB = −2 Hz, GB = 80%) was applied to enhance the spectral resolution.

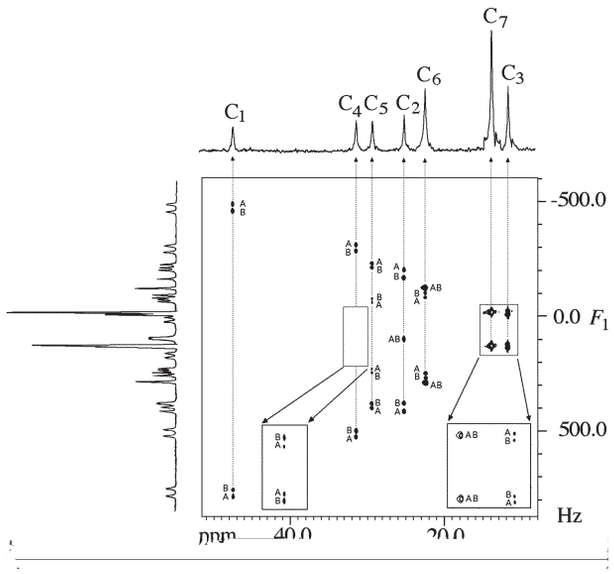

Fig. 3 Carbon–deuterium HETCOR 2D spectrum of (±) -EHA-d_{15} dissolved in the chiral nematic solvent PBLG/$CHCl_3$, recorded at B_O = 9.4 T, of (±)-EHA-d_{15}. The labels A and B refer to the two enantiomers. Inside the 2D plot are displayed two 2D expansions showing doublets associated with the C3, C4 and C7 carbon atoms. The 2D spectrum was acquired in magnitude mode as a 128 (t_1) × 1600 (t_2) data matrix with 512 scans per t_1 increment. The refocussing delays τ and τ' are fixed to 12.5 ms and 4.2 ms, and the recycling delay is 712 ms. A gaussian ($LB_1 = -5$ Hz, $GB_1 = 40\%$) and lorentzian ($LB_2 = 10$ Hz) filtering was used in the F_1 and F_2 dimensions, respectively.

spectrum was assigned by recording a 2D INADEQUATE experiment (not shown) on a sample of the acid dissolved in chloroform. Indeed, the chemical shift differences between the isotropic and the liquid crystal samples are expected to be small and can be neglected for the purpose of assignment.

There is no enantiomeric discrimination in the carbon spectrum, and so this experiment does not assign the doublets at a particular CD_2 site to the separate enantiomers. This assignment was achieved by recording a ^2H–^2H COSY 2D spectrum. The deuterium nuclei in a single enantiomer are coupled through ^2H–^2H dipolar interactions, which produce correlation peaks between deuterium nuclei, even though the splittings from this spin–spin interaction are not resolved in the deuterium 1D spectrum.[9] At this stage the quadrupolar splittings, $\Delta\nu_i^A$ and $\Delta\nu_i^B$ for each site and each enantiomer have been assigned, but not whether the enantiomer is *R* or *S*, and indeed this cannot be done directly from NMR data on a racemic mixture, and so the labels *A* and *B* are used throughout this paper.[4] It remains to obtain the signs of the quadrupolar splittings. This last step was achieved by recording the proton-coupled ^{13}C spectrum of the fully protonated (±)-EHA dissolved in the PBLG/$CHCl_3$ liquid crystalline solvent.[1,10] The concentration of the acid is identical to that of the deuterated sample (within the experimental errors on the weighing), and the full spectrum is shown in Fig. 4.

The individual carbon spectra are dominated by $^1T_{CH}$, the one-bond, total spin–spin coupling, which is related to the scalar and dipolar couplings by[11]

$$^1T_{CH} = {}^1J_{CH} + 2\,{}^1D_{CH} \qquad (3)$$

Longer range proton–carbon couplings serve only to broaden the lines. The proton-coupled carbon spectra are also dependent on scalar and dipolar couplings between the protons. Again, this serves only to produce a line broadening for the peaks for C1, C3 and C7. The peaks given by the methylene carbons are, however, strongly influenced by the coupling between the two attached protons. These protons are

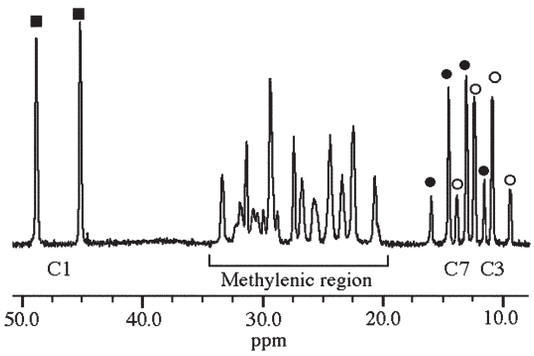

Fig. 4 100.4 MHz proton-coupled carbon-13 1D spectrum of (±)-EHA dissolved in the PBLG/$CHCl_3$ chiral nematic phase at 300 K recorded by adding 10 240 scans of 12 K data points. Proton irradiation during the relaxation delay was used to produce an NOE effect. No filtering was applied. The components of the quadruplets associated with the C3 and C7 methyl groups are labelled with open and black circles, respectively. Signals of the methyne group, C1, are labelled with black squares.

non-equivalent, and hence the carbon-13 spectral patterns are of type ABX. As it can be seen in Fig. 5a, the spectral region associated with the methylene groups is rather congested due to the numerous peak overlaps. To visualize separately the ^{13}C methylene spectral patterns, we have recorded the "T"-resolved 2D spectrum of the (±)-EHA.

The pulse sequence and the 2D spectrum after the double Fourier transformation are identical to the well-known proton–carbon-13 J-resolved experiment used for samples in isotropic solvents.[12] Fig. 5b shows the "T"-resolved 2D spectrum as well as the X part of the various ABX spectral patterns corresponding to the four methylene groups. The spectral patterns observed are very different for the individual methylene groups, due to the differences in magnitude and the sign of $^2D_{HH}$ and $^1D_{CH}$ for each of them.[13] However, for each carbon site there is just one ABX pattern, that is, the signals

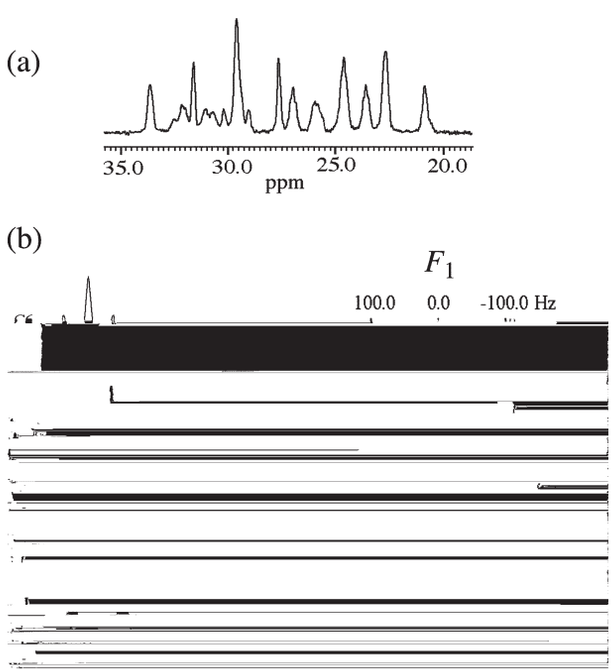

Fig. 5 (a) Expansion of the methylene region of the proton-coupled 100.4 MHz ^{13}C spectrum of (±)-EHA. (b) "T"-resolved 2D spectrum of (±)-EHA acquired in magnitude mode as a 128 (t_1) × 1024 (t_2) data matrix with 80 scans *per* t_1 increment and a recycling delay of 1 s. Proton decoupling is not applied during the second incremented period t_1 of the sequence. No filtering is applied during the F_1 dimension.

from the R and S forms coincide within the experimental linewidths.

The general approach adopted to obtain the signs of the quadrupolar splittings was to produce estimates of the magnitudes of the $^1D_{CH}$. To do this we first note that $^1D_{CH}$ depends on the order parameter of the C–H bond direction, S_{CH}, by[11]

$$^1D_{CH} = -\left(\frac{\mu_o}{4\pi}\right)\left(\frac{\gamma_C\gamma_H h}{4\pi^2 R_{CH}^3}\right)S_{CH} \qquad (4)$$

where μ_0 is the magnetic susceptibility of free space, γ_C and γ_H are magnetogyric ratios, and R_{CH} is the CH bond length averaged over all vibrational motion. The quadrupolar splitting $\Delta\nu_{CD}$ depends on a single order parameter, S_{CD}, if the quadrupolar tensor for the deuterium at this site is axially symmetric about the C–D bond direction.[1,11] Thus,

$$\Delta\nu_{CD} = (3/2)q_{CD}S_{CD} \qquad (5)$$

where q_{CD}, the quadrupolar coupling constant for the deuterium can be assigned a value for an aliphatic C–D site of 170 kHz, with a precision of about 5%. Both experiment and theory suggest that departures from axial symmetry are of the order of 5%. The two order parameters S_{CH} and S_{CD} can be assumed equal to within about 5%, and so the ratio $\Delta\nu/^1D_{CH}$ is approximately independent of the two order parameters, and is equal to

$$\frac{\Delta\nu_{CD}}{^1D_{CH}} = -\frac{24\pi^3 q_{CD}R_{CH}^3}{\mu_o\gamma_C\gamma_H h} \qquad (6)$$

This ratio for aliphatic compounds should lie approximately in the range 10.5–12.0, and a value of 11.5 was chosen in order to get estimates of the magnitudes of the values of $^1D_{CH}$ at the 7 sites in (±)-EHA, and which are summarized in Table 1. Comparing the experimental magnitudes of $^1J_{CH}$ with $^1T_{CH}$ obtained from line separations in the first-order carbon spectra given by sites C1, C3 and C7, provides the signs of $^1D_{CH}$ unambiguously even with the approximations necessary in deriving eqn. (6), and the small possible difference in concentrations of the components in the two liquid crystalline mixtures. In the case of the methylene carbon peaks, it was necessary to simulate the ABX spectra (A, B for protons and X for carbon-13), and to do so requires values for $^2D_{HH}$, $^2J_{HH}$ and δ_{AB}, the chemical shift difference between the two, non-equivalent methylene protons.[13]

The value of $^2J_{HH}$ was taken to be −12 Hz at each site, and δ_{AB} was obtained from the chemical shift differences between the deuteriums at the same site. The observed ABX spectra were compared with those simulated with the two possible signs of the estimated values of $^1D_{CH}$ and with a range of values of $^2D_{HH}$ until a good match was found between simulated and observed spectra. The final step was to iteratively fit the observed and calculated frequencies to produce the magnitudes and signs of these two dipolar couplings, which are given in Table 1. Note that the precision on the spectral data obtained from the carbon spectrum of the fully protonated sample of (±)-EHA is much lower than that on the quadrupolar splittings obtained on the deuterated sample, and the purpose of analyzing the carbon spectra was only to obtain the signs of the $\Delta\nu$.

The structure, conformational distribution and orientational order

In order to apply eqn. (2), it is necessary to invoke a model for describing how the order parameters vary with the conformational state, and it is necessary to use models which involve the molecular mean field approximation.[14] Thus, the molecule of interest is considered to be in the average field from all neighbours. If it is assumed that the orientation of a solute molecule is independent of the distance from the ordered, solvent

Table 1 NMR spectral data for the enantiomers of (±)-EHA recorded at 300 K in the PBLG/$CHCl_3$ chiral nematic phase

Carbon atom	1	2		3	4		5		6		7
Group	CH	CH_2		CH_3	CH_2		CH_2		CH_2		CH_3
^{1}H Numbering	16	14,15		11,12,13	17,18		19,20		21,22		23,24,25
$\delta_{^{13}C}$/ppm	47.14	25.15		11.70	31.43		29.50		22.61		13.86
$\lvert^1D_{CH}\rvert$ (estimated)[a]	109 ± 5	52 ± 5	0 ± 5	13 ± 2	71 ± 5	14 ± 3	53 ± 5	27 ± 5	36 ± 5	29 ± 5	13 ± 2
$^1D_{CH}$ (fitted)	119 ± 5	50 ± 5	-5 ± 5	12 ± 2	75 ± 5	8 ± 2	52 ± 5	21 ± 2	31 ± 5	31 ± 5	13 ± 2
$\delta_{^2H}$/ppm	2.26	1.61	1.51	0.90	1.61	1.46	1.28		1.27		0.85
$\Delta\nu^A$/Hz[b]	−1289	−620	0[c]	−161	−838	−140	−626	−299	−416	−333	−147
$\Delta\nu^B$/Hz[b]	−1222	−544	0[c]	−139	−780	−180	−598	−316	−416	−359	−147
Spectral discrimination	y	y	n	y	y	y	y	y	n	y	n
$\lvert\Delta\nu^A - \Delta\nu^B\rvert$/Hz	67	76	0	22	58	40	28	17	0	26	0

[a] The estimated value of $\lvert^1D_{CH}\rvert$ derived from the average of $\lvert\Delta\nu\rvert$ measured for the two enantiomers. Such a calculation is possible if we assume that the differential ordering effect between two enantiomers is small as is the case for the PBLG solvent. [b] The *S* and *R* descriptors are replaced by the arbitrary notation *A* and *B*. The precision of the measurement for the non-zero quadrupolar splittings is estimated at ±2 Hz. [c] The precision on this value is ±5 Hz.

molecules, then it is possible to represent $U_{ext}(\beta,\gamma,\phi_i)$, the average, orientational energy for the molecule in a conformation specified by the angles ϕ_i, as an infinite series in spherical harmonics, and for uniaxial phases, such as the chiral nematic PBLG/$CHCl_3$ system, it is sufficient to use an expansion in modified spherical harmonics, $C_{L,m}(\beta,\gamma)$:

$$U_{ext}(\beta,\gamma,\phi_i) = -\sum_{L,m\,even} \varepsilon_{L,m}(\phi_i) C_{L,m}(\beta,\gamma) \qquad (7)$$

where β and γ are the polar angles made by the mesophase director in a molecule-fixed frame, which is a principal frame for the interaction tensor $\varepsilon_{L,m}(\phi_i)$.

The total, average energy, $U_{LC}(\beta,\gamma,\phi_i)$, of the flexible solute must also contain a term, $U_{int}(\phi_i)$, which is independent of the orientation of the molecule in the liquid crystalline phase, and which is determined by the form of the various bond rotation potentials. Thus, we can write[15]

$$U_{LC}(\beta,\gamma,\phi_i) = U_{ext}(\beta,\gamma,\phi_i) + U_{int}(\phi_i) \qquad (8)$$

The order parameters $S_{\alpha\beta}$ are related to averages, $\langle C_{2,m}\rangle$, of the second-rank spherical harmonics:

$$\begin{aligned} S_{zz} &= \langle C_{2,0}\rangle \\ S_{xx} - S_{yy} &= \sqrt{(3/2)}(\langle C_{2,2}\rangle + \langle C_{2,-2}\rangle) \\ S_{xy} &= i\sqrt{(3/8)}(\langle C_{2,2}\rangle - \langle C_{2,-2}\rangle) \\ S_{xz} &= i\sqrt{(3/8)}(\langle C_{2,-1}\rangle + \langle C_{2,1}\rangle) \\ S_{yz} &= i\sqrt{(3/8)}(\langle C_{2,1}\rangle - \langle C_{2,-1}\rangle). \end{aligned}$$

The conformationally-dependent order parameters, $S_{\alpha\beta}(\phi_i)$, are then similarly related to averages, $\langle C_{2,m}(\phi_i)\rangle$ of $C_{2,m}(\beta,\gamma)$, where β and γ are polar angles for the director in a frame fixed in the molecule when it is in the conformation defined by the ϕ_i. The averages are determined by

$$\langle C_{2,m}(\phi_i)\rangle = Q(\phi_i)^{-1} \int_0^{\pi} \sin\beta \mathrm{d}\beta \times \int_0^{2\pi} \mathrm{d}\gamma C_{2,m}(\beta,\gamma) \exp[-U_{ext}(\beta,\gamma,\phi_i)/k_BT] \qquad (9)$$

with

$$Q(\phi_i) = \int_0^{\pi} \sin\beta \mathrm{d}\beta \int_0^{2\pi} \mathrm{d}\gamma \exp -[U_{ext}(\beta,\gamma,\phi_i)/k_BT]. \qquad (10)$$

For cases where the orientational order of the solute molecules is weak, the condition $U_{ext}(\beta,\gamma,\phi_i) \ll k_BT$ holds for normal temperatures, and so the exponential term in eqns. (9) and (10) can be replaced by $[1 - U_{ext}(\beta,\gamma,\phi_i)/k_BT]$, and invoking eqn. (7) gives

$$\langle C_{2,m}(\phi_i)\rangle = Q(\phi_i)^{-1} \int_0^{\pi} \sin\beta \mathrm{d}\beta \int_0^{2\pi} \mathrm{d}\gamma\, C_{2,m}(\beta,\gamma) \times [1 + \sum_{L,m\,even} \varepsilon_{L,m}(\phi_i) C_{L,m}(\beta,\gamma)/k_BT], \qquad (11)$$

and

$$Q(\phi_i) = \int_0^{\pi} \sin\beta\, \mathrm{d}\beta \int_0^{2\pi} \mathrm{d}\gamma [1 + \sum_{L,m\,even} \varepsilon_{L,m}(\phi_i) C_{L,m}(\beta,\gamma)/k_BT]. \qquad (12)$$

The integrals to be evaluated are of three types:

(a) $\int_0^{\pi} \sin\beta\,\mathrm{d}\beta \int_0^{2\pi} \mathrm{d}\gamma C_{L,m}(\beta,\gamma) = 0$;

(b) $\int_0^{\pi} \sin\beta\,\mathrm{d}\beta \int_0^{2\pi} \mathrm{d}\gamma C_{2,m}(\beta,\gamma) C_{L,m}(\beta,\gamma) = 0$ when $L \neq 2$, and $= 4\pi/5$ for $L = 2$;

(c) $\int_0^{\pi} \sin\beta\,\mathrm{d}\beta \int_0^{2\pi} \mathrm{d}\gamma = 4\pi$.

Eqn. (11), therefore, simplifies to

$$\langle C_{2,m}(\phi_i)\rangle = \frac{\varepsilon_{2,m}(\phi_i)}{5k_BT}. \qquad (13)$$

This means that the second-rank order parameters are determined only by the second-rank terms in the general expansion of the mean potential (eqn. (7)).

To progress further it is necessary to adopt a model for the conformational dependence of the interaction coefficients. We have chosen to adopt the additive potential model,[11,14] which approximates the $\varepsilon_{2,m}(\phi_i)$ as sums of contributions, $\varepsilon_{2,p}(j)$, from bonds, or rigid sub-units of the molecules, thus

$$\varepsilon_{2,m}(\phi_i) = \sum_{j,p} \varepsilon_{2,p}(j) D^2_{p,m}(\omega_{j,\phi_i}). \qquad (14)$$

The Wigner functions, $D^2_{p,m}(\omega_{j,\phi_i})$, describe the orientation of fragment *j* in the molecular reference frame, when the molecule is in the conformation specified by the ϕ_i.

Calculation of the molecular geometry and bond rotation potentials

To calculate the quadrupolar splittings it is necessary to adopt a set of interaction parameters, $\varepsilon_{2,p}(j)$, a molecular geometry,

and a form for each of the bond rotation potentials, $V(\phi_i)$. There is insufficient experimental data to obtain optimized values of all of these quantities by fitting the calculated to observed quadrupolar splittings. Consequently it was necessary to assume a molecular geometry which is independent of the conformational state, and to vary only the $\varepsilon_{2,p}(j)$, and parameters dependent on the bond rotation potentials. There are no published structures of this acid, or of any closely related compound, and so the structure has been predicted by a molecular orbital calculation. This was done by the Hartree–Fock method with a gaussian basis set of type 6-311G(d,p), as implemented in the Gaussian 98 program suite.[16] The first step was to calculate a structure for the molecule in the lowest energy conformation. This structure has C4 to C7 lying approximately in a plane which is twisted by 4° out of the plane defined by C1, C2 and C3. The bond angles and bond lengths are given in Table 2. The positions of the secondary minima, the *gauche* + and − states (denoted below as g^+ and g^-), for C–C–C–C fragments in a straight chain hydrocarbon are symmetrically placed about the *trans* state ($\phi = 0°$), and in calculations on such chains they are usually assumed to be at positions $\phi = \pm 112°$. In contrast, rotations about the CC bonds in a chain containing a chiral C atom will in principle be such that the two *gauche* forms are now expected to be inequivalent in energy, and at positions not related by symmetry. This was explored for each of the C–C bonds in the chiral acid. To do this an initial series of calculations for each bond rotation was done by the Hartree–Fock method with a smaller basis set, 6-31G, and with the bond lengths and angles fixed at values found by optimization with the molecules fixed in the all-*trans* form. In these calculations, for example to explore $V_{12}(\phi_1)$, the molecular structure was held fixed in the all-*trans* structure except for rotation of atoms 3,11,12,13,14 and 15 about the C1–C2 bond. The *gauche* forms were found to be close to positions ±120° from the *trans* state, and so calculations with the extended 6-311G(d,p) basis set were started from these positions, and geometry optimization used in a search for local minima. This gave the results shown in Table 2. These calculations predicted that the g^+ and g^- states are related by a mirror plane only for rotation about C5–C6.

Fig. 6 shows the rotamers as Newman projections, together with the calculated relative energies. The geometries do change on rotation about the bonds, and the angles ϕ given in Fig. 6 are for the rotation of the appropriate C atom, and are relative to the *trans* rotamer.

Fitting the two sets of data by the AP method

The probability, $P_{LC}(\phi_{ij})$, that the molecule is in a conformation in the liquid crystalline phase specified by the bond rotation angles ϕ_{ij} is given by

$$P_{LC}(\phi_{ij}) = Z^{-1} \int \sin\beta \, d\beta \, d\gamma \exp[-U_{LC}(\beta, \gamma, \phi_{ij})/k_B T] \quad (15)$$

with

$$Z = \int \sin\beta \, d\beta d\gamma \, d\phi_{ij} \exp[-U_{LC}(\beta, \gamma, \phi_{ij})/k_B T] \quad (16)$$

The probability, $P_{iso}(\phi_{ij})$, that the molecule is in a conformation in the isotropic phase specified by the values of ϕ_{ij} is given by

$$P_{iso}(\phi_{ij}) = \exp[-U_{int}(\phi_{ij})/k_B T] / \int \exp[-U_{int}(\phi_{ij})/k_B T] d\phi_{ij}. \quad (17)$$

For a liquid crystalline phase with low orientational order, as is the case here, $P_{LC}(\phi_{ij})$ is identical with $P_{iso}(\phi_{ij})$. The conformations considered are only those generated by rotation

Table 2 Bond lengths and angles of (±)-EHA in the minimum energy, all-*trans* and the *gauche* + and *gauche* − forms calculated by the method HF-6-311G(d,p) in the Gaussian 98 package. The *gauche* forms are for rotations about one bond only, denoted by $g^{\pm}(i,j)$. An entry in the table occurs only if the geometrical parameter was optimized in the rotamer, otherwise the geometry is the same as in the optimised all-*trans* rotamer. The dihedral angles are defined as in Gaussian 98, so that a *trans* arrangement of four atoms occurs at 180°

Rotamer	Atom p	Atom q	r_{pq}/pm	Atom s	Angle pqs/deg	Atom t	Angle pqst/deg
All-*trans*	C2	C1	153.7				
All-*trans*	C3	C2	152.9	C1	114.18		
All-*trans*	C4	C1	153.7	C2	111.40	C3	184.0
$g^+(1,2)$							−77.3
$g^-(1,2)$							46.2
$g^+(4,5)$					110.42		
$g^-(4,5)$					111.12		184.11
All-*trans*	C5	C4	153.0	C1	114.37	C2	175.3
$g^+(1,4)$							74.4
$g^-(1,4)$							−48.8
$g^+(4,5)$					116.95		163.2
$g^-(4,5)$					115.98		179.13
All-*trans*	C6	C5	153.0	C4	112.80	C1	182.30
$g^+(4,5)$					116.38		70.94
$g^-(4,5)$					115.10		296.83
$g^+(5,6)$					114.77		
$g^-(5,6)$					114.74		
All-*trans*	C7	C6	152.7	C5	113.05	C4	180.17
$g^+(4,5)$					112.37		172.99
$g^-(4,5)$					112.63		185.33
$g^+(5,6)$							70.26
$g^-(5,6)$							290.9
All-*trans*	C8	C1	151.5	C2	109.60	C3	62.40
$g^+(4,5)$					108.56		61.74
$g^-(4,5)$					109.59		62.63
All-*trans*	O9	C8	132.9	C1	113.32	C2	242.10
All-*trans*	O10	C8	118.4	C1	124.71	C2	61.88
All-*trans*	H11	C3	108.7	C2	110.51	C1	177.42
All-*trans*	H12	C3	108.7	C2	111.29	C1	57.60
All-*trans*	H13	C3	108.7	C2	111.73	C1	−63.08
All-*trans*	H14	C2	108.7	C1	107.70	C4	−54.40
$g^+(1,2)$					108.71		50.02
$g^-(1,2)$					109.41		173.59
All-*trans*	H15	C2	108.7	C1	108.70	C4	61.16
$g^+(1,2)$					109.14		165.32
$g^-(1,2)$					107.58		−71.46
All-*trans*	H16	C1	108.7	C2	109.09	C3	−55.23
$g^+(4,5)$					109.06		−55.59
$g^-(4,5)$					108.70		−54.82
All-*trans*	H17	C4	108.7	C1	108.68	C2	−61.70
$g^+(1,4)$							196.04
$g^-(1,4)$							73.67
$g^+(4,5)$					108.70		−71.52
$g^-(4,5)$					108.10		−58.36
$g^+(5,6)$					108.83		
$g^-(5,6)$					107.97		
All-*trans*	H18	C4	108.7	C1	107.76	C2	53.85
$g^+(1,4)$							−49.00
$g^-(1,4)$							188.51
$g^+(4,5)$					106.79		42.89
$g^-(4,5)$					107.65		56.68
$g^+(5,6)$					107.09		
$g^-(5,6)$					107.90		
All-*trans*	H19	C5	108.7	C4	109.85	C1	65.71
$g^+(4,5)$					109.24		−62.65
$g^-(4,5)$					108.69		−53.85
$g^+(5,6)$					109.42		61.46
$g^-(5,6)$					110.21		60.05
All-*trans*	H20	C5	108.7	C4	109.42	C1	−55.81
$g^+(4,5)$					108.12		52.28
$g^-(4,5)$					109.40		61.09

Table 2 (continued)

Rotamer	Atom p	Atom q	r_{pq}/pm	Atom s	Angle pqs/deg	Atom t	Angle pqst/deg
$g^+(5,6)$					109.76		−55.12
$g^-(5,6)$					108.99		−56.52
All-*trans*	H21	C6	108.7	C5	109.28	C4	58.16
$g^+(4,5)$					109.33		51.23
$g^-(4,5)$					110.04		63.63
$g^+(5,6)$					109.01		−52.89
$g^-(5,6)$					108.54		169.10
All-*trans*	H22	C6	108.7	C5	109.20	C4	−57.84
$g^+(4,5)$					110.21		−65.64
$g^-(4,5)$					109.24		−53.00
$g^+(5,6)$					108.61		−167.98
$g^-(5,6)$					109.03		54.02
All-*trans*	H23	C7	108.7	C6	111.17	C5	180.03
All-*trans*	H24	C7	108.7	C6	111.17	C5	−59.94
All-*trans*	H25	C7	108.7	C6	111.13	C5	60.04
All-*trans*	H26	O9	94.6	C8	108.18	O10	0.06

between the minimum energy forms, as shown in Fig. 6, and the conformational distribution is therefore characterized by 7 parameters: $E_{tg}^{+}(i,j)$ and $E_{tg}^{-}(i,j)$ for $i,j = 1,2$; 1,4; and 4,5, and $E_{tg}^{\pm}(5,6)$, whilst the positions of the energy minima are kept constant. There are 11 observed quadrupolar splittings, and so only 4 other parameters can be safely varied in the AP method in order to fit calculated to observed splittings. The AP method requires values of interaction parameters $\varepsilon_{2,m}(j)$ for suitable rigid molecular fragments. These were chosen to be ε_{C-C}, ε_{C-H}, ε_{C-O}, and $\varepsilon_{C=O}$. It is important to note that these tensor components are not independent variables, and hence their optimized values do not have a direct physical significance, but simply represent one way of modeling the total interaction tensor and its conformational dependence.

The conformational distribution was approximated as the set of minimum energy structures produced by independent rotations about the four bonds C1–C2, C1–C4, C4–C5, C5–C6 between *trans* and *gauche* ± states. Rotations about bonds C2–C3 and C6–C7 were assumed to have 3-fold symmetry. The bond C1–C8 was considered to be fixed. Calculations were done with a 2-fold symmetry for this bond rotation, but this had no effect on the quality of the fit of observed to calculated data, and served only to change the best-fit values of ε_{C-O} and $\varepsilon_{C=O}$.

The first step was to assign the two quadrupolar splittings observed in each enantiomer for each of the four methylene groups in the *A* form of the acid. To do this all 16 possible assignments of two splittings at 4 sites were used with the AP calculations, in each case determining the optimum values of the 7 $E_{tg}(i,j)$ and the 4 bond interaction parameters.

The use of 11 variables to fit 11 observed splittings does not necessarily lead to a perfect fit because the variables are not linearly independent, and there were large differences in the quality of the fit obtained for the 16 data assignments, as measured by RMS, the root mean square error:

$$\mathrm{RMS} = \{\sum [\Delta\nu_i(\mathrm{observed}) - \Delta\nu_i(\mathrm{calculated})]^2/11\}^{1/2} \quad (18)$$

Five assignments were judged to be acceptable on the basis of the value of *R*, however, only one of these assignments gave the all-*trans* form as the lowest energy conformer, and this was therefore chosen as the correct assignment, and is that shown in Table 3.

Note that the best fit between observed and calculated splittings for the correct assignment was obtained using the geometry calculated by the MO method, rather than if a model geometry was used. The next step was to repeat these calculations on the data for the B enantiomer. The structure of enantiomer B was constructed to be a mirror image of A with respect to the *xz* plane, and the conformational distribution was at first assumed to be related to that of A by reversing the signs of $E_{tg}^{+}(i,j)$ and $E_{tg}^{-}(i,j)$. The quadrupolar splittings were then fitted to those observed by varying only the four values of $\varepsilon_{2,0}^{B}(j)$. This gave a reasonable fit only for the assignment shown in Table 3, with a value of RMS = 17 Hz. The calculations were then repeated but allowing the rotamer energy differences to vary as well as the bond interaction parameters, to give a much closer fit to the data, with an RMS = 6 Hz. The observed and calculated quadrupolar splittings are compared in Table 3, whilst the values of $E_{tg}^{\pm}$ and $\varepsilon_{2,0}(j)$ are shown in Table 4.

Finally, the quadrupolar splittings for both enantiomers were fitted simultaneously with one set of conformational parameters, which are the averages of those which gave the best individual fits to the two data sets, and two separate sets of values of the bond interaction parameters, with the results shown in Tables 3 and 4.

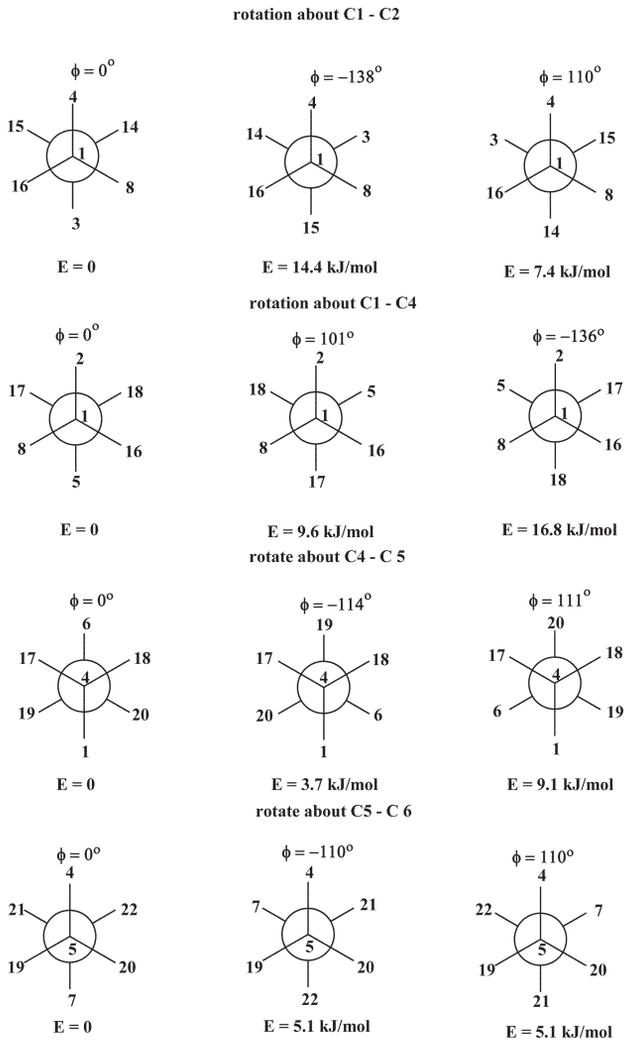

Fig. 6 Rotamers generated by rotation about the C–C bonds in EHA, together with the relative energies calculated by the molecular orbital method HF/6-311G(d,p). In these rotamers, the other flexible parts are in the *trans* position. The angles of rotation ϕ are for the appropriate C atom, and are relative to these atoms being in a *trans* arrangment.

The conformational distributions

For the enantiomers to have identical conformational distributions, then $E_{tg}^{+}(i,j)$ for *A* should equal $E_{tg}^{-}(i,j)$ for *B*, and *vice*

Table 3 Best fit obtained between observed quadrupolar splittings for the two enantiomers of (±)-EHA-d_{15} dissolved in the chiral nematic solvent PBLG/$CHCl_3$, and values calculated by the AP method

	Enantiomer *A*			Enantiomer *B*		
Atom	$\Delta\nu$/Hz observed	$\Delta\nu$/Hz calculated[a]	$\Delta\nu$/Hz calculated[b]	$\Delta\nu$/Hz observed	$\Delta\nu$/Hz calculated[a]	$\Delta\nu$/Hz calculated[b]
16	−1289	−1290	−1293	−1222	−1222	−1219
14	−620	−627	−627	−544	−549	−552
15	0	−4	−5	0	−3	−8
11	−161	−156	−151	−139	−136	−145
17	−838	−827	−822	−780	−769	−773
18	−140	−135	−132	−180	−175	−181
19	−299	−301	−307	−316	−321	−315
20	−626	−634	−626	−598	−606	−615
21	−416	−409	−417	−416	−409	−397
22	−333	−338	−351	−359	−359	−346
23	−147	−151	−151	−147	−151	−152
RMS/Hz	—	7	10	—	6	11

[a] All 7 $E_{tg}^{\pm}$ and 4 bond interaction parameters varied. [b] The $E_{tg}^{\pm}$ values kept fixed at the average of the values found by calculations of type (a) for both enantiomers, and only the values of the four bond interaction parameters were varied.

versa, and this is clearly not the case for the values derived by the AP calculations when all 11 parameters are allowed to vary, as shown in Table 4. There are 81 conformers even in our simplified model, most of them of low probability. However, the main features of the distributions can be seen by comparing the probability of the all-*trans* form with those which have just one *gauche* link. This is done in Table 5 which has the 14 most populated conformers for the two enantiomers. Note that for enantiomer *A* the conformer with one g^- (g^+ for enantiomer *B*) configuration about the C1–C4 bond is absent: it has essentially zero probability for all the distributions. The most striking feature of the probability distributions is the large differences between the distributions determined from the NMR data and those calculated by the HF/6-311G(d,p) method. The MO method predicts much smaller probabilities of conformations involving *gauche* forms, and hence the probability of the all-*trans* conformer is much larger (0.588) than for the AP derived values (0.099–0.134).

A second major difference is that the MO method finds $E_{tg}^{+}(4,5) > E_{tg}^{-}(4,5)$, whilst the opposite is determined by the AP calculations. This leads to a reversal in relative values of $P_{iso}(0,111,0,0)$ and $P_{iso}(0,-114,0,0)$ predicted by the MO and AP methods.

One important reason why the values of $E_{tg}^{+}(i,j)$ and $E_{tg}^{-}(i,j)$ obtained from the MO and AP calculations are not the same is because the MO calculations done here are for particular points along a bond rotation path, whereas the quadrupolar splittings are averages over the whole path. The AP method employed here assumes the average can be calculated from only three points on the path. Clearly, this difference in the two ways of obtaining the values of $E_{tg}^{+}(i,j)$ and $E_{tg}^{-}(i,j)$ will most probably yield different values. It is to be expected that the AP method will underestimate the importance of the *trans* configurations, as is observed. However, the MO calculations done here for the values of $E_{tg}^{+}(i,j)$ and $E_{tg}^{-}(i,j)$ considered only one structure, that in which rotation occurs only for a single bond, the rest of the molecule is in the *trans* conformation. In contrast, the AP method is deriving values for the bond C_i–C_j which are averages over the effects of changing the conformation about all other bonds in the molecule. In other words, the AP method is sensitive to possible correlations between the bond rotations, whilst the particular MO calculations are not. To explore such correlations by the molecular orbital method would require doing a full geometry optimisation on the 81 minimum energy structures, which was not a practical possibility.

Table 4 The energy differences, $E_{tg}^{+}(i,j)$ and $E_{tg}^{-}(i,j)$, and the bond interaction parameters, ε_{XY}, for enantiomers *A* and *B* found by fitting quadrupolar splittings to those calculated by the AP method. The molecular orbital (MO) values for the energy differences are also given

	AP calculations				
	Enantiomer *A*		Enantiomer *B*		MO calculations Enantiomer *A*
	a	*b*	*a,c*	*b,c*	
$E_{tg}^{+}(1,2)$/kJmol^{-1}	1.75	1.68	1.87	2.69	7.4
$E_{tg}^{-}(1,2)$/kJmol^{-1}	3.51	2.69	1.61	1.68	14.4
$E_{tg}^{+}(1,4)$/kJmol^{-1}	1.17	0.93	46.6	45.70	9.6
$E_{tg}^{-}(1,4)$/kJmol^{-1}	44.8	45.70	0.68	0.93	16.8
$E_{tg}^{+}(4,5)$/kJmol^{-1}	2.88	3.01	4.38	4.51	9.1
$E_{tg}^{-}(4,5)$/kJmol^{-1}	4.64	4.51	3.14	3.01	3.7
$E_{tg}^{\pm}(5,6)$/kJmol^{-1}	2.12	1.93	1.76	1.93	5.1
ε_{CC}/kJmol^{-1}	0.0579	0.0586	0.0581	0.0594	—
ε_{CH}/kJmol^{-1}	0.0217	0.0207	0.0200	0.0219	—
ε_{CO}/kJmol^{-1}	−0.0215	−0.0227	−0.0200	−0.0180	—
$\varepsilon_{C=O}$/kJmol^{-1}	0.0354	−0.00117	−0.0102	−0.0322	—

[a] Varying all 11 parameters. [b] $E_{tg}^{\pm}$ values fixed at the averages of the values found for the two enantiomers from calculations of type (a). [c] Note that E_{tg}^{+} for enantiomer *B* are to be compared with E_{tg}^{-} for enantiomer *A*, and *vice versa*.

Table 5 The 14 most populated rotamers of the two enantiomers *A* and *B* of (±)-EHA determined by fitting the experimental quadrupolar splittings by the AP method and allowing all 11 parameters to vary for (a) enantiomer *A*, and (b) for enantiomer *B* and (c) having an identical conformational distribution for *A* and *B*

					$P_{iso}(\phi_{56},\phi_{45},\phi_{14},\phi_{12})$[a]			
Rotamer	ϕ_{56}	ϕ_{45}	ϕ_{14}	ϕ_{12}	(a)	(b)	(c)	MO
1	0	0	0	0	0.134	0.099	0.113	0.588
2	0	0	101	0	0.079	0.075	0.078	0.013
3	0	0	0	110	0.065	0.052	0.058	0.031
4	110	0	0	0	0.056	0.049	0.052	0.076
5	−110	0	0	0	0.056	0.049	0.052	0.076
6	0	111	0	0	0.041	0.028	0.034	0.015
7	0	0	101	110	0.039	0.040	0.040	0.0006
8	−110	0	101	0	0.034	0.037	0.036	0.002
9	110	0	101	0	0.034	0.037	0.036	0.002
10	0	0	0	−138	0.032	0.045	0.039	0.002
11	110	0	0	110	0.028	0.037	0.027	0.004
12	−110	0	0	110	0.028	0.037	0.027	0.004
13	0	111	101	0	0.025	0.021	0.023	0.0003
14	0	−114	0	0	0.020	0.017	0.019	0.134

[a] Normalised for the 81 rotamers.

Note that the disagreement between $E_{tg}^{-}(1,4)$ calculated to be ~45 kJmol^{-1} by the AP method and ~17 kJmol^{-1} by the MO method is not important. In both cases these values imply a virtually zero probability for conformations involving this *gauche* state. In fact, the values obtained by the AP method are more realistically determined to be $\gtrsim$ 15 kJ mol^{-1}.

The orientational order parameters

The orientational order parameters for a flexible molecule in a liquid crystalline phase are dependent on the conformational state, and so a full description in the simplified conformational model involves 81 matrices. One simple way of showing that the orientational order does differ for the two enantiomers is to compare the averages:

$$S_{\alpha\beta} = \sum_n S_{\alpha\beta}(n) \qquad (19)$$

Over the *n* discrete conformations, and these values are given in Table 6. Another simplified comparison is to compare the order parameters of the all-*trans* conformer, as shown in Table 7.

Conclusion

We have shown that it is possible to assign the quadrupolar splittings in the deuterium spectrum of a sample of (±)-EHA-d_{15} dissolved in a chiral nematic solvent, and to determine the absolute signs of these splittings. The methodology used to do this can be applied to other, deuterated achiral molecules.

The data obtained were then used to explore the relationship between the conformational distribution and orientational order of the two enantiomers. To do this it is necessary to adopt a model for how the orientational order depends on the conformational state of the molecules, and this was done using a molecular mean field approximation for the anisotropic interaction potential between an EHA molecule and the PBLG helices. The additive potential model adopted approximates this potential as a sum of contributions from interactions between bonds in the EHA molecules and the mean field from the PBLG molecules. It was also necessary to adopt

Table 6 Orientational order parameters, $S_{\alpha\beta}$, averaged over the conformational distributions for enantiomers *A* and *B* of EHA dissolved in the PBLG/$CHCl_3$ chiral nematic solvent. The data are for the results of AP calculations which (a) allow each enantiomer to have a different conformational distribution, and (b) which constrain both enantiomers to have an identical conformational distribution

	(a)		(b)	
	Enantiomer *A*	Enantiomer *B*	Enantiomer *A*	Enantiomer *B*
S_{zz}	0.00305	0.00210	0.00227	0.00276
$S_{xx}-S_{yy}$	−0.00406	−0.00106	−0.00109	−0.00391
S_{xy}	0.00393	−0.00383	0.00402	−0.00379
S_{xz}	−0.00013	−0.00024	−0.00021	−0.00018
S_{yz}	−0.00036	0.00047	−0.00043	0.00042

Note that in a common axis system *xyz*, no enantiomeric differentiation occurs when $S_{zz}(A) = S_{zz}(B)$, $S_{xx}(A) - S_{yy}(A) = S_{xx}(B) - S_{yy}(B)$, $S_{xy}(A) = -S_{xy}(B)$, $S_{xz}(A) = S_{xz}(B)$ and $S_{yz}(A) = -S_{yz}(B)$.

a simplified model for the conformational distribution, and this was to assume that the molecules exist only in a set of minimum energy conformations. The results obtained by treating the NMR data with this approximate procedure has two important features. Firstly that the conformational distributions obtained for both enantiomers differ considerably from that calculated by the HF/6-311G(d,p) molecular orbital method. This may simply reflect the differences in the two ways of obtaining the energy differences $E_{tg}^{\pm}(i,j)$. The MO calculations done here obtain these by comparing the energies of the molecule in three conformations generated by rotating about the bond C_i–C_j whilst keeping the rest of the molecule fixed in the all-*trans* conformation. A partial geometry optimization was done for each of the three conformations. The AP method, however, uses a geometry which was kept fixed at that obtained by the MO calculations for the all-*trans* structure, and calculates the quadrupolar splittings, as an average over the three minimum energy positions, and this can be expected to overestimate the derived values of $E_{tg}^{\pm}(i,j)$. The MO calculations are also for single, isolated molecules, whereas the AP results are for the molecules in a liquid environment. Secondly, the AP calculations which give the best fits to the NMR data produce significantly different conformational distributions for the two enantiomers. This is certainly not impossible, but in view of the approximate nature of the calculations this result should be regarded with caution. It is difficult to judge how the various assumptions in the AP model affect this result, and the precision of the values of $E_{tg}^{\pm}(i,j)$ can only be determined by carrying out a realistic computer simulation of this complex liquid crystalline phase, which is not practicable with current computing power.

Table 7 Orientational order parameters, $S_{\alpha\beta}$(all-*trans*) for the all-*trans* conformer for enantiomers *A* and *B* of EHA dissolved in the PBLG/$CHCl_3$ chiral nematic solvent. The data are for the results of AP calculations which (a) allow each enantiomer to have a different conformational distribution, and (b) which constrain both enantiomers to have an identical conformational distribution

	(a)		(b)	
	Enantiomer *A*	Enantiomer *B*	Enantiomer *A*	Enantiomer *B*
S_{zz}(all-*trans*)	0.00571	0.00547	0.00537	0.00571
($S_{xx}-S_{yy}$) (all-*trans*)	−0.00198	0.00165	0.00139	−0.00158
S_{xy}(all-*trans*)	0.00380	−0.00376	0.00390	−0.00368
S_{xz}(all-*trans*)	0.00029	0.00025	0.00027	0.00029
S_{yz}(all-*trans*)	0.00004	−0.00003	−0.00004	−0.00004

The AP calculations also show that the orientational order of the two enantiomers are different, which is not surprising, and has been found for many rigid solutes.[6]

Acknowledgements

JWE acknowledges the award of a Senior Emeritus Fellowship from the Leverhume Trust. The authors wish to thank Prof. Jacques Courtieu for many helpful discussions.

References

1 M. Sarfati, P. Lesot, D. Merlet and J. Courtieu, *Chem. Commun.*, 2000, 2069.
2 C. Aroulanda, S. Sarfati, J. Courtieu and P. Lesot, *Enantiomer*, 2001, **6**, 2081.
3 P. Lesot, D. Merlet, M. Sarfati, J. Courtieu, H. Zimmermann and Z. Luz, *J. Am. Chem. Soc.*, 2002, **124**, 10071; A. Parenty, J.-M. Campagne, C. Aroulanda and P. Lesot, *Org. Lett.*, 2002, **4**, 1663.
4 P. Lesot, M. Sarfati and J. Courtieu, *Eur. Chem. J.*, 2003, **9**, 1725.
5 J. W. Emsley, in *NMR of Liquid Crystals*, ed. J. W. Emsley, Riedel, 1985.
6 P. Lesot, Y. Gounelle, D. Merlet, A. Loewenstein and J. Courtieu, *J. Phys. Chem.*, 1995, **99**, 14871; P. Lesot, D. Merlet, T. P. Rantala, J. Jokisaari, J. W. Emsley and J. Courtieu, *J. Phys. Chem. A*, 1997, **101**, 5719.
7 J. W. Emsley, in *Encyclopedia of NMR*, eds. D. M. Grant and R. K. Harris, John Wiley & Sons, Chichester, 1995, p. 2781.
8 H. Zimmermann, *Liq. Cryst.*, 1989, **4**, 591.
9 P. Lesot, M. Sarfati, D. Merlet, B. Ancian, J. W. Emsley and B. A. Timimi, *J. Am. Chem. Soc.*, 2003, **125**, 7689.
10 (*a*) P. Lesot, D. Merlet, A. Meddour, A. Loewenstein and J. Courtieu, *Faraday Trans.*, 1995, **91**, 1371; (*b*) A. Meddour, P. Berdagué, A. Hedli, J. Courtieu and P. Lesot, *J. Am. Chem. Soc.*, 1997, **119**, 4502.
11 J. W. Emsley, in *Encyclopedia of NMR*, eds. D. M. Grant and R. K. Harris, John Wiley & Sons, Chichester, 1995, p. 2788.
12 S. Braun, H.-O. Kalinowski and S. Berger, in *150 and More Basic NMR Experiments*, Wiley-VCH, Weinheim, 1998; A. Bax, *Two-Dimensional Nuclear Magnetic Resonance in Liquids*, Delft University Press, Dordrecht, 1984.
13 M. Edgar, J. W. Emsley and M. I. C. Furby, *J. Magn. Reson.*, 1997, **128**, 105.
14 J. W. Emsley, G. R. Luckhurst and C. P. Stockley, *Proc. R. Soc. London Ser. A*, 1982, **381**, 117.
15 J. W. Emsley and G. R. Luckhurst, *Mol. Phys.*, 1980, **41**, 19.
16 Gaussian 98, Revision A.7, Inc., Pittsburgh, P.A., 1998.

